Draft version January 14, 2022
Typeset using LaTeX **twocolumn** style in AASTeX631

The family of V1311 Ori: a young sextuple system or a mini-cluster?

Andrei Tokovinin[1]

[1] *Cerro Tololo Inter-American Observatory — NSF's NOIRLab Casilla 603, La Serena, Chile*

ABSTRACT

A compact bound group of four active M-type dwarfs containing V1311 Ori is identified in the Gaia catalog of nearby stars. Located at a distance of 39 pc, it is likely related to the β Pictoris and 32 Ori moving groups by kinematics, isochronal age, and other indicators of youth (Hα emission, presence of lithium, and fast rotation). The brightest star A is a known close binary, for which a preliminary 80-yr visual-spectroscopic orbit is determined. Star B is resolved here into a $0\farcs08$ pair, and the faintest stars C and D are probably single. Considering the non-hierarchical configuration with projected separations of $\sim$10 kau, this could be either a young sextuple system or a bound but dynamically unstable mini-cluster (trapezium) that avoided disruption so far. This pre-main-sequence system bridges the gap between moving groups and wide hierarchies.

Keywords: binary stars — multiple stars — pre-main-sequence stars — moving clusters

1. INTRODUCTION

Star formation is a story of concentration and dispersal, of inward (collapse) and outward (jets and outflows) gas motions. Young stars follow the pattern by condensing into small groups and clusters which later disperse, leaving behind bound stellar systems and single stars. The hierarchical collapse can last for 10–30 Myr at the largest spatial scales, but it is much faster at small scales (Vázquez-Semadeni et al. 2019).

Young moving groups (YMGs), such as β Pictoris (BPMG), witness a transition from concentration to dispersal. Their members still stay together in space and preserve coherent galactic motion. However, smaller aggregates of stars, such as wide pairs and multiples, may be in the process of disintegration caused by their internal dynamics, and in this regard are similar to dispersing young clusters. A relatively frequent occurrence of wide pairs (compared to the field) in the BPMG and in other YMGs is well documented (Caballero 2010; Alonso-Floriano et al. 2015; Elliott & Bayo 2016). Although the abundance of wide pairs in the YMGs is uncontestable, their status is uncertain: they could be a mix of long-lived bound binaries and small unstable disintegrating groups of stars. Ultra-wide pairs are even more frequent in the 1-Myr old Taurus star-formation region (Joncour et al. 2017); they trace the primordial clustering and are still in the concentration, rather than dispersal, phase.

Here I study a group of four co-moving stars in the solar neighborhood, called V1311 Ori system after its brightest member. It has been identified by search of hierarchies in the Gaia Catalog of Nearby Stars, GCNS (Gaia Collaboration et al. 2021a). Some of these young and chromospherically active stars were studied individually as potential members of YMGs and for other reasons, but the fact that they form a gravitationally bound group has, so far, escaped attention. The brightest stars A and B are close pairs, so the system contains at least six components. A triangular configuration on the sky (Figure 1) with comparable separations between A, BC, and D suggests that this system might be non-hierarchical, hence dynamically unstable, which makes it particularly interesting. As shown below, currently available information does not allow a conclusive choice between the two options, so this system could be either a marginally stable hierarchy or a disintegrating mini-cluster. The first option is illustrated by the mobile diagram in Figure 2.

Section 2 summarizes main chracteristics of these stars and some published results relevant to the nature and dynamics of the group. In section 3.1 I report new high-resolution imaging which resolved the subsystem Ba,Bb and allowed determination of the preliminary visual-spectroscopic orbit of Aa,Ab. Photometric variability,

andrei.tokovinin@noirlab.edu

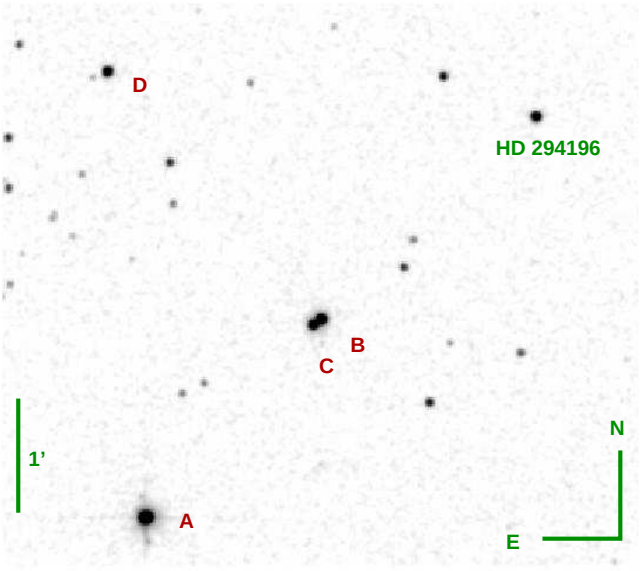

Figure 1. Location of the four stars on the sky. The underlying image is from 2MASS band K (Skrutskie et al. 2006). The object is 2° north of the Orion nebula.

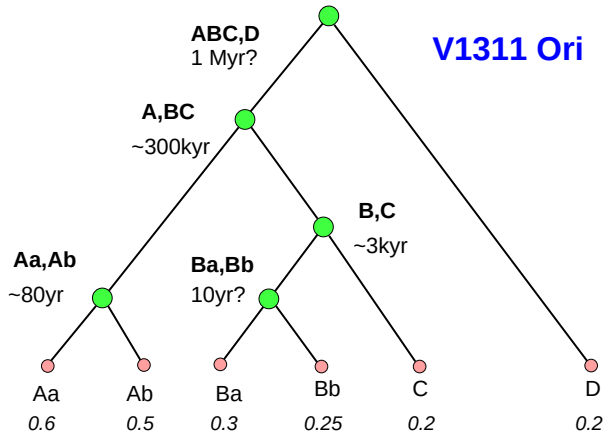

Figure 2. Possible hierarchy of the V1311 Ori system. The numbers in italics are estimated masses of the components.

rotation, and emission lines are briefly covered in section 3.3. Then in section4 the internal motions in this system and its relation to YMGs are investigated. Discussion of the results in section 5 closes the paper.

2. MAIN PARAMETERS AND LITERATURE

The four co-moving stars, designated as A-D in order of decreasing brightness, were found in the GSNS. Their mutual projected distances are within the radius of 10 kau imposed in the initial search (Tokovinin 2022). To probe for other, more distant members of this system, I searched the full Gaia Early Data Release (EDR3) catalog (Gaia Collaboration et al. 2021b) around V1311 Ori with a radius of 5° and a constraint on parallax $\varpi > 20$ mas. The search returned 84 objects. Filtering on the proper motion (PM) reduces this selection to five stars. The additional fifth star, called here component E, is known as RX J0534.0-0221 or TIC 427346731, and it is another well-studied member of BPMG. The angular distance between E and A is 52′ (0.6 pc), but E is closer to the Sun than ABCD by 4 pc (parallax 29.12±0.03 mas). So, E is another member of the moving group, but it is not bound to the V1311 Ori system.

Table 1 contains coordinates and other parameters of the components, including star E for completeness. The first two lines give the Simbad and 2MASS (Skrutskie et al. 2006) identifiers. The coordinates (equinox J2000, epoch 2016.0), parallaxes, and PMs are from Gaia EDR3. The Reduced Unit Weight Error (RUWE) parameter indicates the quality of Gaia astrometric solutions, being normally below 1.4 for single stars. Elevated values of RUWE for A and B are caused by motion in the inner subsystems Aa,Ab and Ba,Bb, not accounted for in the Gaia 5-parameter astrometric solutions. This reduces the accuracy of parallaxes and biases the PMs. For this reason, the long-term PM of star A from Tycho-2 (Høg et al. 2000) is preferred over the biased short-term PM from Gaia; unfortunately, no accurate long-term PM is available for B. The radial velocities (RVs) are taken from various sources.

The historical reasons to study these stars were their young age (manifested by X-ray detections and Hα emission), their potential membership in YMGs, or their proximity to the Sun. Finch et al. (2014) looked for stars within 25 pc from the Sun using the UCAC4 astrometric catalog. They list star D as UPM 0532-0303 and star B as PM 05319-0303W and estimate their distances as 20.7 and 16.3 pc, respectively, based on photometric criteria (these young stars are brighter compared to normal dwarfs, causing under-estimated distances). The stars were subsequently included in the program of astrometric monitoring. Its results, reported by Vrijmoet et al. (2020), contain components A, B, C under a common name UPM0531-0303 and with common coordinates, causing confusion. In fact, their components A, B, and C correspond to our stars B, C, and D (Vrijmoet, 2021, private communication). The measured parallaxes, similar to the Gaia ones, move these stars outside the 25-pc horizon of their program. No astrometric perturbations were noted in the data spanning 3.3 years.

The youth of V1311 Ori is manifested by the Hα emission in its spectrum and by its X-ray detection. However, originally the star was attributed to the pre-main-

Table 1. Data on components of the V1311 Ori system

Parameter	A	B	C	D	E
Simbad ID	V1311 Ori	PM 05319-0303W	...	ESO-HA 737	RX J0534.0-0221
2MASS	05320450-0305291	05315786-0303367	05315816-0303397	05320596-0301159	05335981-0221325
R.A. (EDR3)	05:32:04.51	05:31:57.88	05:31:58.17	05:32:05.97	05:33:59.83
Dec. (EDR3)	-03:05:30.0	-03:03:37.6	-03:03:40.7	-03:01:16.8	-02:21:33.3
ϖ (mas)[a]	27.22±0.58[b]	26.30±0.09	25.91±0.02	25.96±0.02	29.11±0.03
μ^*_α (mas yr^{-1})	6.6±3.1[b]	17.62 (4.2)	8.14	8.06	9.53
μ_δ (mas yr^{-1})	-51.1±3.2	-51.79	-54.02	-50.66	-58.41
RUWE	33.50	3.95	1.32	1.23	1.21
RV (km s^{-1})	22.2±0.3[c]	23.1±1.0[d]	...	23.6±2.7[d]	21.09±0.02[e]
Spectral type	M1.5V	M4.5	...	M5	M3
V (mag)	11.437	13.855	14.89	15.61	12.42
G (mag)	10.442	12.701	13.241	13.912	11.267
J (mag)	7.88	9.45	10.11	10.58	8.56
K_s (mag)	7.01	8.54	9.22	9.70	7.70

[a] PMs and parallaxes from Gaia EDR3 (Gaia Collaboration et al. 2021b).

[b] PM from Tycho-2 (Høg et al. 2000)

[c] RV of the center of mass Aa,Ab

[d] RV from Bell et al. (2017)

[e] RV from Fouqué et al. (2018)

sequence (PMS) population of the background Orion association, until da Silva et al. (2009), Malo et al. (2013), and others considered V1311 Ori as a candidate member of BPMG. However, Elliott et al. (2014) refuted the BPMG membership on the basis of RV (biased by the orbital motion of Aa,Ab). Bell et al. (2017) took spectra of stars B+C (blended) and D, which they denoted as THOR 33 and THOR 34, respectively. They attributed these stars to the 32 Ori (THOR) moving group which has age and kinematics similar to the BPMG and is located at a mean distance of 93 pc, much further than our system. They detected strong Hα emission in both stars, measured their RVs, and noted that D had broad lines. The two RVs of D measured within a year agreed, suggesting that it is a fast rotator rather than a close binary. Durkan et al. (2018) took five high-resolution spectra of V1311 Ori in 2011-2015, measured accurate RVs, and detected an RV trend. Their results are incorporated in the orbital solution for Aa,Ab presented below.

Figure 3 shows the color-magnitude diagrams (CMDs) for the members of V1311 Ori family and star E in the $M_V, V-K$ and Gaia colors. The contribution of companions to the light of A and B has been subtracted. The stars align reasonably well on the 24 Myr solar-metallicity isochrone from Bressan et al. (2012), matching the age of BPMG and THOR groups (Bell et al. 2015, 2017). The masses estimated from the isochrone are 0.60, 0.26, 0.23, and 0.17 $M_\odot$ for Aa-D, respectively.

3. INNER SUBSYSTEMS

3.1. *Speckle Interferometry*

The components of this system were observed with high angular resolution at the 4.1 m Southern Astrophysical Research Telescope (SOAR) in 2021 October-December. The instrument and data processing are covered in (Tokovinin 2018). Briefly, series of 400 images with exposure time of 28 ms and a pixel scale of 15 mas are recorded as image cubes and processed by the standard speckle interferometry method, computing the spatial power spectrum, auto-correlation function, and shift-and-add image (co-added with centering on the brightest pixel). Two data cubes per observation are normally recorded and processed independently. The stars were observed here with the I filter transmitting wavelengths from 725 to 895 nm (at half-maximum, including the detector response); the effective wavelength is longer than 824 nm for these red stars. The diffraction-limited resolution is about 40 mas.

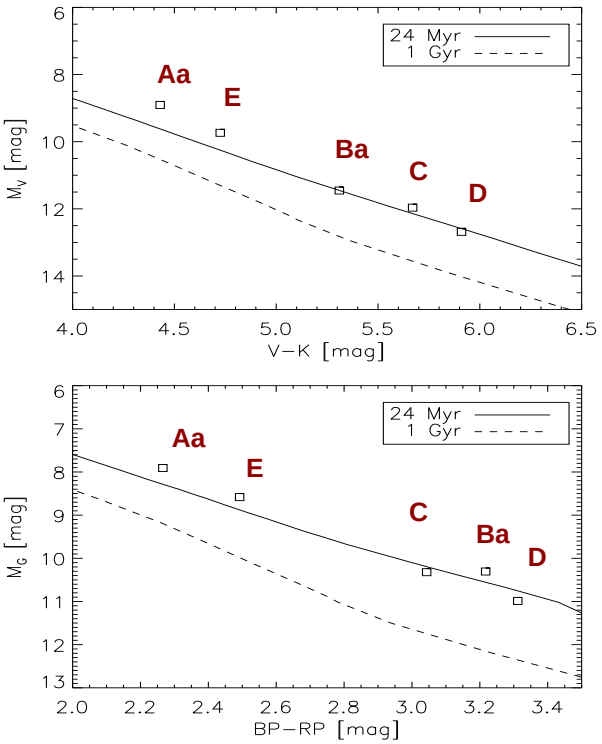

Figure 3. Color-magnitude diagrams. The full and dashed lines are PARSEC isochrones (Bressan et al. 2012) for 24 Myr and 1 Gyr, respectively.

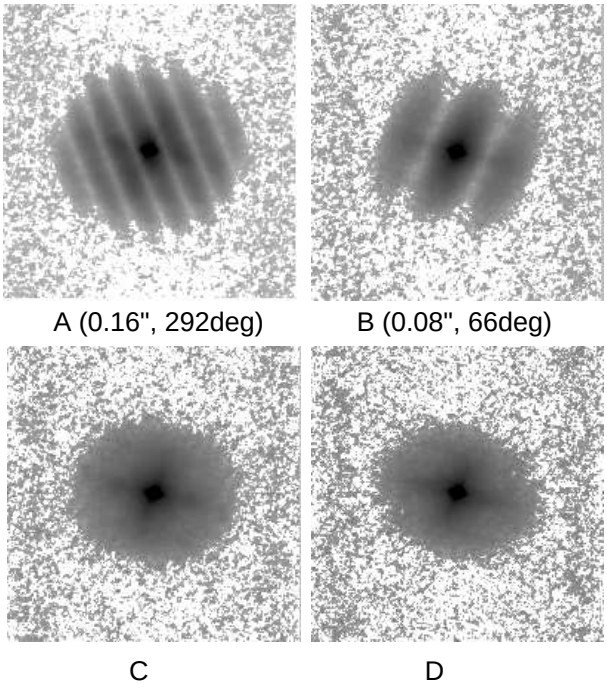

Figure 4. Speckle power spectra of the four stars (in negative logarithmic rendering) recorded on 2021 November 19 at SOAR. Fringes in the spectra of A and B indicate that they are resolved close pairs, while C and D do not have companions with separations above 0.″04.

Table 2. Speckle interferometry of V1311 Ori

Pair	Date	θ	ρ	ΔI
	(JY)	(deg)	(arcsec)	(mag)
Aa,Ab	2021.7983	291.3	0.1578	0.97
Aa,Ab	2021.8857	292.3	0.1655	0.87
Aa,Ab	2021.9596	292.9	0.1711	0.86
Ba,Bb	2021.8857	66.3	0.0816	0.52
Ba,Bb	2021.8910	65.5	0.0772	0.59
Ba,Bb	2021.9596	67.0	0.0824	0.55

Star A was pointed and resolved on 2021 October 18 (2021.80). This pair is listed in the Washington Double Star Catalog (Mason et al. 2001) as JNN 39. It has been resolved for the first time by Janson et al. (2012) and later confirmed by Janson et al. (2014). On 2021 November 19 (2021.89), I observed all four stars, taking advantage of extremely good 0.″5 seeing. Star B was also resolved as a tight binary, while stars C and D were point sources. Figure 4 shows the speckle power spectra. The faint stars B, C, D were recorded with a 50 ms exposure, A — with the standard 28 ms exposure. The pair Ba,Bb was re-measured two days later to confirm its resolution, and both pairs were measured again on December 16 (2021.96). All SOAR speckle measurements of Aa,Ab and Ba,Bb are given in Table 2. The random errors of relative positions are 5 mas or less. The quadrants of both pairs are determined without the 180° ambiguity. The separation of Aa,Ab increases over two months in agreement with the orbit presented below.

3.2. *The Orbit of Aa,Ab*

The projected separation of Aa,Ab corresponds to an orbital period on the order of 20 yr. Although the published measurements (Janson et al. 2012, 2014) and the SOAR speckle interferometry cover only part of the orbit, its general character is already clear. The pair has passed through the periastron in 2019 and now is opening up again.

After fitting positional measurements by a set of preliminary elements, I included the RVs as additional constraints and fitted them jointly with positions using the IDL code `ORBIT` (Tokovinin 2016a). The RV data are described in the following section. The position measurements and RVs still do not constrain the orbit well enough and can be fitted by a family of orbits with pe-

Table 3. Two orbits of V1311 Ori Aa,Ab (JNN 39)

Orbit	P	T	e	a	Ω_A	ω_A	i	K_1	γ
	(yr)	(yr)		(arcsec)	(deg)	(deg)	(deg)	(km s^{-1})	(km s^{-1})
1	80	2019.35	0.778	0.499	133.2	47.6	63.0	3.52	22.20
2	143	2019.56	0.854	0.807	132.5	45.6	67.8	3.88	21.76

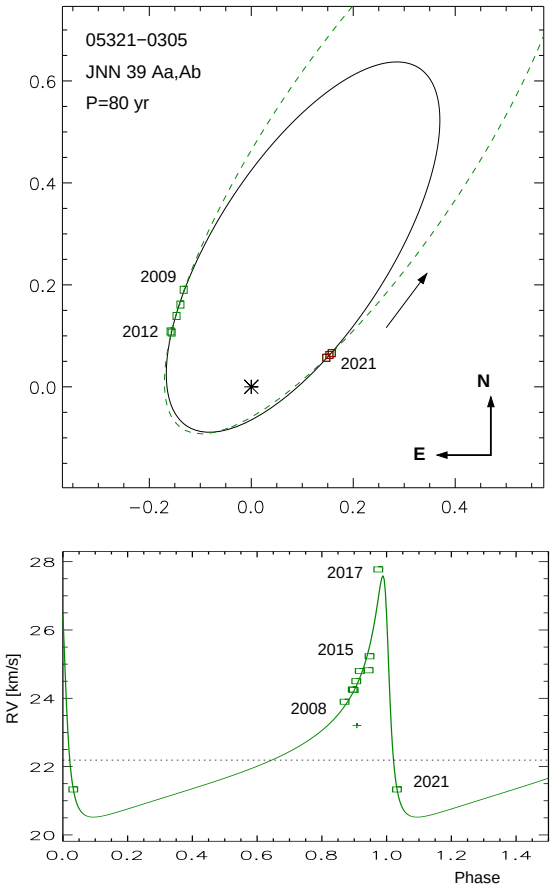

Figure 5. Tentative visual and spectroscopic orbit of Aa,Ab (orbit 1). The upper panel shows position measurements with scale in arcseconds (the SOAR measurements in 2021 are plotted in red, those of Janson et al. in green). The dashed line shows the alternative long-period orbit 2. The lower panel is the RV curve (the dotted line shows the systemic velocity, the cross marks the rejected measurement).

riods ranging from ∼40 yr to over a century. Two representative orbits from this family are listed in Table 3 in common notation. The preferred 80-yr orbit 1 (Figure 5) is obtained by fixing the incination to 63°, to obtain the expected mass sum of 1.1 $M_\odot$ for a parallax of 26 mas. The second orbit 2 with $P = 143$ yr and a larger eccentricity results from the unconstrained fit and corresponds to the mass sum of 1.45 $M_\odot$, larger than estimated. The fitted elements and their errors depend on the adopted data errors, (5 and 2 mas for position measurements, 0.4 km s^{-1} for RVs), so the large formal errors of the elements are esentially meaningless. Some elements, e.g. the periastron time T and the node position angle Ω_A, are already well defined by the data. The systemic velocity γ of 22.20±0.28 km s^{-1} derived for the preferred 80-yr orbit 1 is adopted as the RV of star A. The weighted rms residuals to both orbits are 1 mas in positions and 0.3 km s^{-1} in RV, less than the estimated measurement errors.

The orbit predicts that in 2016.0 Ab moved relative to Aa with the speed of $(-10.3, -33.4)$ mas yr^{-1} in RA and Dec, respectively. The difference between the short-term PM of A measured by Gaia EDR3 and the long-term PM in Tycho-2 is $(3.5, 11.0)$ mas yr^{-1}. The direction of the PM difference matches the expected reflex motion of the photo-center and suggests that its amplitude is a factor of $f \approx 0.33$ smaller than the semimajor axis. The estimated masses of Aa and Ab (0.6 and 0.5 $M_\odot$) and the magnitude difference of 0.9 mag measured at SOAR correspond to $f = 0.15$. This factor increases to $f = 0.22$ if a larger $\Delta m = 1.3$ mag measured by Janson et al. (2012) is adopted.

The orbital inclination, RV amplitude, and the mass of Aa correspond to the mass of 0.38 $M_\odot$ for Ab, somewhat smaller than estimated from the absolute magnitude and the isochrone. Considering the preliminary nature of the Aa,Ab orbit, it is premature to investigate further these minor disagreements between the photo-center motion, RV amplitude, and estimated masses. Although the distance to the system is known quite well, the orbit is not yet useful for testing evolutionary models of low-mass PMS stars.

3.3. *Photometry and Spectroscopy*

Stars A and B are present in the TESS input catalog as TIC 50745582 and 50745567, respectively. Their fluxes were monitored by the TESS satellite (Ricker et al. 2014) in sectors 6 (2018 November) and 32 (2020 November). I extracted the light curves from the MAST archive; their 3-day fragments are plotted in Figure 6. Star A shows an almost perfect sinusoidal variation with

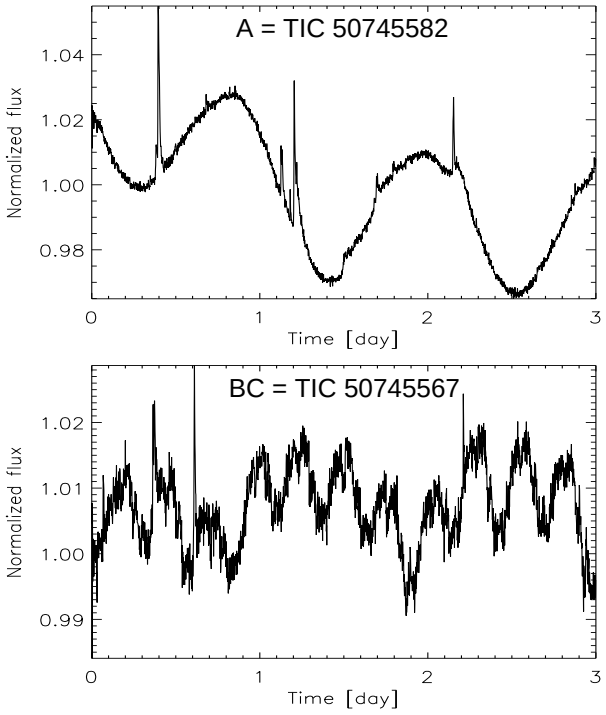

Figure 6. Fragments of the light curves of stars A and BC recorded by TESS in sector 32 (2020 November). The first point is at JD 2459174.2234.

a period of 1.119 days and an amplitude of 0.020 (a weak second harmonic is detectable in the 2020 data), with frequent flares. There is a second period of 4.37 days with an amplitude of 0.015, previously detected from ground-based photometry by Messina et al. (2017), so A is a multi-periodic M-dwarf as defined by Rebull et al. (2018). The flux variation of star B (blended with C) has the main period of 0.2642 days (6.34 h), implying rotation near the breakup speed, similar to some young low-mass stars studied by Rebull et al. The light curve is not sinusoidal, resembling scallop-type variable late-M dwarfs identified by Stauffer et al. (2017). The flux of BC recorded by TESS corresponds to at least three stars Ba, Bb, and C. The period of 1.119 days is also detectable in the flux of BC with an amplitude of 0.005, presumably due to contamination from star A located at 148″ from BC.

In the orbital fit, I used five RVs measured by Durkan et al. (2018) from high-resolution spectra taken with FEROS (Fiberfed Extended Range Optical Spectrograph) on the ESO-MPG 2.2 m telescope from 2010.9 to 2015.098. I also found in the ESO archive another FEROS spectrum taken on JD 2457855.5019 (2017.279) and measured the RV of 27.77 km s^{-1} by cross-correlation. Three RVs from table C.3 of Elliott et al. (2014) are also used (the first one in 2008.9), although

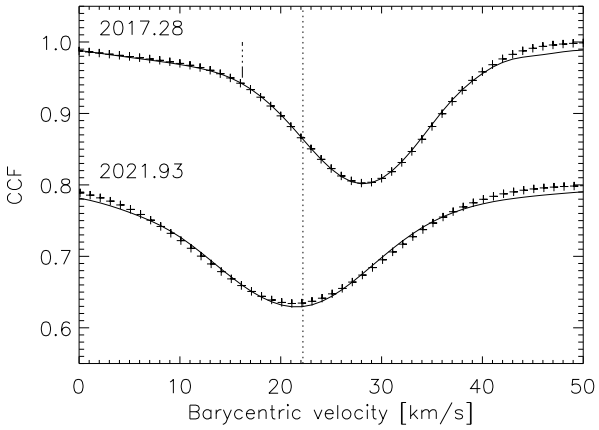

Figure 7. CCFs of the FEROS and CHIRON spectra of V1311 Ori (full lines) and their Gaussian approximations (crosses). The CHIRON CCF is displaced vertically by −0.2. The vertical dotted line marks the systemic velocity of Aa,Ab, the short dash-dot line corresponds to the expected RV of the secondary component in 2017.28.

one discrepant RV (JD 2455904.18) is excluded from the fit (cross in the lower panel of Figure 5). I re-computed the RV from that spectrum and obtaied a similar result, suggesting a problem with wavelength calibration.

A contemporary spectrum of V1311 Ori was taken on 2021 December 6 (JD 2459555.7431) using the CHIRON high-resolution optical spectrometer on the Cerro Tololo 1.5 m telescope, operated by the SMARTS consortium. The instrument and data processing are described in (Tokovinin et al. 2013; Paredes et al. 2021). The spectrum was acquired in the fiber mode with a resolution of 27,000 and an exposure time of 15 min. The RV of 21.33 km s^{-1} was determined by computing the cross-correlation function (CCF) with a binary mask based on the solar spectrum (see details in Tokovinin 2016b). Figure 7 shows the CCFs for the last FEROS spectrum taken in 2017.27 (near the peak of the RV curve) and the CHIRON spectrum. Both have one dip with an rms width of 7.49 and 9.13 km s^{-1}, respectively (the CHIRON spectrum has a lower resolution compared to FEROS). The dip width implies a projected rotation velocity $V \sin i$ of 12 km s^{-1}; da Silva et al. (2009) also measured a rotation velocity of 12 km s^{-1}.

A star like Aa with a 0.77 $R_\odot$ radius (inferred from the isochrone) rotating at a 1.119 day period has an equatorial velocity of 34 km s^{-1}. The CCF dip indicates a rotation three times slower and matches the longer photometric period of 4.37 days. Most likely, star Ab is a fast rotator responsible for the 1.119-day period. Its broad and low-contrast dip is not detected in the 2017 CCF at the expected velocity of 16.2 km s^{-1} (the short line in Figure 7), despite the moderate magnitude difference

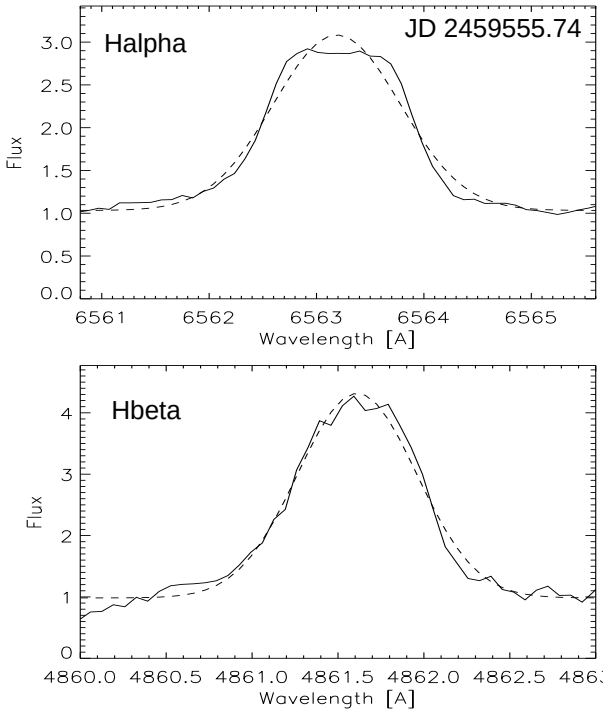

Figure 8. Hydrogen emission lines in the CHIRON spectrum (full lines) and fitted Gaussians (dashed lines).

between Aa and Ab measured by speckle interferometry. However, this CCF does have a slight asymmetry and it was tentatively fitted by two Gaussians (crosses), with Ab rotating at ∼20 km s^{-1} and having a dip contrast of 0.03. Unfortunately, the dips of Aa and Ab are heavily blended now and will remain blended for decades, until the next periastron.

Spectrum of star B was taken with CHIRON on 2021 December 22 (JD 2459571.6361). Its CCF has a shallow and wide dip corresponding to the RV of 17.5±1 km s^{-1} and an rms width of 28 km s^{-1}, or $V \sin i \sim 55$ km s^{-1}. I also correlated this spectrum with synthetic spectra of late-M dwarfs to confirm these measurements. The photometric period of 0.2462 days detected in BC corresponds to an equatorial speed of 112 km s^{-1} (for a 0.55 $R_\odot$ radius). Low-resolution spectra of BC and D taken by Bell et al. (2017) show very broad lines in D, rather than in BC, but the CHIRON spectrum of B confirms its fast rotation; the lines of Ba and Bb are totally blended. Orbital motion of Ba,Bb should cause the RV variation.

Several authors noted other signs of youth in the spectra of stars A, B, and D, namely presence of the lithium line and a strong emission in the Balmer hydrogen lines. Figure 8 shows these emissions in the CHIRON spectrum of A. The equivalent widths of Hα and Hβ are −3.13 and −2.78 Å, respectively, their FWHMs are 1.39 and 1.86 Å (85 km s^{-1}). The CHIRON spectrum of V1311 Ori also shows chromospheric emission in the cores of the sodium D lines. In the FEROS spectra, the equivalent width of Hα varies from −3.72 to −2.75 Å, and its double-peaked profile is slightly asymmetric, with the maximum on the left side. A strong Hα emission is present in the CHIRON spectrum of B.

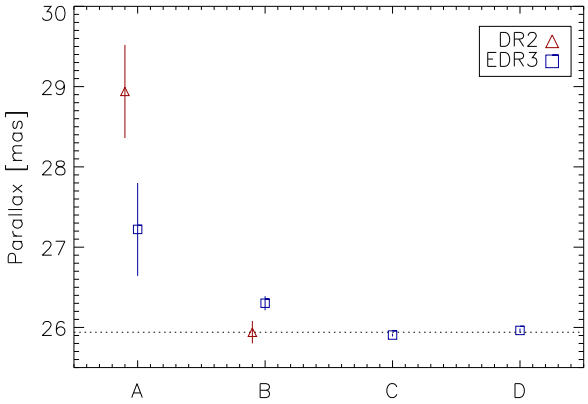

Figure 9. Parallaxes of four stars in Gaia EDR3 and DR2. The dotted line marks the mean parallax of C and D, 25.94 mas.

4. HIERARCHY OR CLUSTER?

In this Section, two alternative views of the V1311 Ori family are presented. The choice depends on the reliability of Gaia parallaxes of stars A and B. The EDR3 parallaxes of the four stars seem to be measurably different (Figure 9). Taking the average parallax of C and D, 25.94 mas, as the best estimate of the distance to the system (38.55 pc), the parallax of A is lager by 1.28±0.58 mas. This formally significant (2.2σ) difference translates to the distance of A 1.8±0.8 pc closer than C and D. However, Gaia DR2 measured for A an even more discrepant parallax of 28.94±0.58 mas. The inconsistency between two Gaia data releases indicates a problematic astrometry, also corroborated by the large RUWE. During the 2014.6-2017.4 period covered by the EDR3, the photocenter of A moved almost linearly in declination, but its motion in RA had a substantial acceleration of 1.4 mas yr^{-2} according to the Aa,Ab orbit. Fitting the 5-parameter solution (position, PM, and parallax) to this non-linear motion, sampled by the Gaia scanning law, inevitably biases the parallax. I tried to reproduce this effect, but found a much smaller (<0.1 mas) bias. My toy model also failed to explain the difference between DR2 and EDR3 parallaxes of A. The Gaia data release 3 will account for accelerations and, hopefully, will give a more trustworthy parallax of A. Cases where Gaia parallaxes of stars in wide physical binaries appear

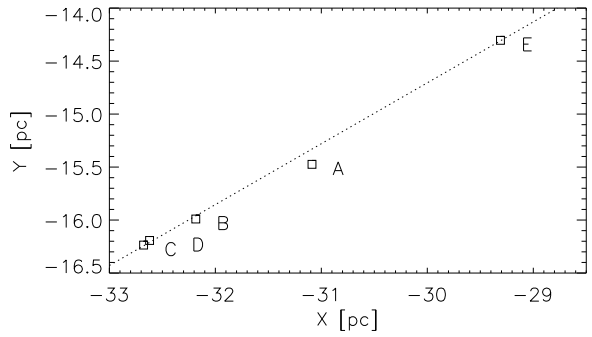

Figure 10. Location of stars A to E projected onto the Galactic plane, assuming their EDR3 parallaxes. The dotted line is a linear fit.

different because one of them contains an unresolved subsystem are not rare.

The parallax of B should also be biased by the Ba,Bb subsystem. However, a smaller RUWE, a better agreement between the two Gaia data releases (the DR2 parallax of B is 25.94±0.14 mas), and a smaller difference from the mean parallax of C and D indicate that the problem is less severe, compared to star A. The orbital period of Ba,Bb estimated from its projected separation is on the order of 10 yr, and the actual period can be longer or shorter by 2-3 times. If the period is only a few years, the impact of the subsystem on astrometry is substantially reduced by time averaging. Although the EDR3 parallax of B differs from the mean parallax of C and D by 0.36±0.09 mas, I attribute this formally significant discrepancy to the bias.

4.1. *A String?*

Suppose for the moment that the Gaia EDR3 parallaxes of A and B can be trusted, implying different distances to these stars. Then their close location on the sky is a mere projection, while the actual configuration in space is a line pointing toward the Sun (Figure 10). In such case, the system cannot be gravitationally bound, and there is no reason to exclude from it star E. Kounkel & Covey (2019) found that young stars are often arranged in linear configurations, strings. However, their strings extend over tens and hundreds of pc.

It appears highly improbable that four cluster members accidentally arranged themselves along our line of sight. Even if this were true, there should be other members of this cluster around, but I found only star E within a 5° search radius. Therefore, the V1311 Ori family (excluding star E) must be a gravitationally bound multiple system, and its configuration in Figure 10 does not correspond to reality.

4.2. *Internal Motions*

Table 4. Internal kinematics of V1311 Ori

Pair	ρ (arcsec)	θ (deg)	s (au)	$\Delta\mu$ (mas yr^{-1})	μ^*
B,C	5.31	125.5	205	9.73 (4.53)	9.72
A,BC	148.5	318.6	5724	8.15 (1.81)	2.91
ABC,D	217.5	16.3	8385	2.00 (0.86)	2.51
A,D	254.2	4.9	9799	1.53	1.86
C,D	185.5	39.1	9799	3.36	1.41

At the distance of 39 pc, the PM of 1 mas yr^{-1} corresponds to 0.18 km s^{-1}. In principle, accurate Gaia astrometry can measure relative tangential motions in V1311 Ori with a high precision, enabling study of its internal kinematics. However, the Gaia PMs of A and B are biased by inner subsystems. The less accurate long-term PM of star A from Tycho-2 (Table 1) matches the PMs of other stars, and its difference with the short-term Gaia PM approximately matches the orbital motion of Aa,Ab (section 3.2). However, the orbit of Ba,Bb is not known yet, and its PM has not been measured by Tycho-2. UCAC4 gives the PM of B as (4.2±6.6, −34.8±4.9) mas yr^{-1}, while Vrijmoet et al. (2020) measured for B (their component A) a PM of (14.5±6.4, −50.5±2.9) mas yr^{-1} on a 3.3 yr time base. The PM of B measured by Gaia DR2 and EDR3 is mutually consistent to within 1 mas yr^{-1}; it is adopted here, despite an almost certain but unknown bias. In contrast, the EDR3 astrometry of C and D can be trusted. Their small RUWE and matching RVs speak against subsystems, although cannot rule them out.

Neglecting the discrepant parallaxes of A and B, I postulate that all four stars are located at a common distance of 38.55 pc. The PM bias of A and B caused by their subsystems is the largest remaining uncertainty in the study of the internal kinematics; another is related to the estimated masses. Despite these caveats, we can evaluate whether this system can be bound or not.

Assume a binary on a circular face-on orbit with a period P and an angular separation (semimajor axis) ρ. Its orbital speed (in arcsec yr^{-1}) is

$$\mu^* = (2\pi\rho)/P = 2\pi\rho^{-1/2}\varpi^{3/2}M^{1/2}, \qquad (1)$$

where ϖ is the parallax in arcseconds, M is the mass sum in solar units, and the third Keler's law is used, $P = (\rho/\varpi)^{3/2}M^{-1/2}$. The characteristic speed μ^* is a scaling factor for binaries with arbitrary eccentricity and orbit orientation. In a bound binary with negative total energy, the relative speed $\Delta\mu$ is always less than $\sqrt{2}\mu^*$. This is a necessary (but not sufficient) condition of boundness.

Table 5. Galactic motion

Star	U	V	W
	km s^{-1}		
A	−14.1	−16.4	−10.2
B	−14.8	−18.2	−9.0
C	−14.5	−17.7	−10.7
D	−15.2	−17.4	−10.5
E	−13.1	−16.6	−9.5
BPMG	−10.9	−16.0	−9.0
THOR	−12.8	−17.7	−9.0

Adopting the masses of 1.1, 0.50, 0.23, and 0.17 $M_\odot$ for stars A, B, C, and D, I computed the mass-weighted positions and PMs of various combinations, their relative motion $\Delta\mu$, and the characteristic speed μ^*. Representative results are given in Table 4. In brackets, $\Delta\mu$ is computed using the UCAC4 $\mu^*_\alpha = 4.2$ mas yr^{-1} for B instead of 17.62 mas yr^{-1} measured by Gaia EDR3. The 5.″3 pair B,C is likely close in space (not only in projection). Its relative motion does not contradict the bound status regardless of the adopted μ^*_α of star B. However, a similar test applied the A,BC pair indicates that it can be bound with the UCAC4 PM of B, but is unbound with the EDR3 PM. The widest combination ABC,D looks bound in both cases. The two lowest-mass stars C and D with accurate astrometry cannot be a bound pair, which is natural (C moves too fast because it revolves around B). On the other hand, A,D could be a wide bound pair (in fact triple) that projects on to another bound triple B,C.

The hierarchical structure shown in Figure 2 assumes that D is the outer component in this sextuple system. Its distance from ABC along the line of sight must be at least 15 kau to ensure the dynamical stability (the accurate parallaxes of C and D indeed imply such distance difference, with a low significance). Even considering the line-of-sight distance of D, the tangential motion of D relative to ABC is slow enough for a bound system. Alternatively, this system can be dynamically unstable. With an estimated outer period of ∼1 Myr, it could have survived for several crossing times and might disrupt in the future.

4.3. *Galactic Motion*

Using data on individual stars from Table 1 (including E), I compute the Galactic velocities U, V, W (the U axis points toward the Galactic center) and list the result in Table 5. The unknown RV of C is assumed to equal the mean RV of the system. Mean velocities of the BPMG and THOR moving groups are given for reference, according to Gagné et al. (2018). The internal velocity dispersion in these groups is about 1 km s^{-1}, and their mean velocities also differ between authors by similar amounts. V1311 Ori is located at Galactic coordinates $(l, b) = (206.^\circ5, -19.^\circ0)$, roughly in the anti-center direction, so the RV errors affect mostly the U component. The velocities of the four stars, computed independently of each other, are mutually consistent and closer to THOR than to BPMG. Given the similar kinematics and age of both YMGs, they are likely related to a common star formation region, to which V1311 Ori also belonged (Gagné et al. 2021). Both the kinematics and the isochrones confirm the age of ∼24 Myr for the V1311 Ori group.

Motion with a relative velocity of 1 km s^{-1}, typical for YMGs, corresponds to 1 pc Myr^{-1}, so stars born together have little chance to stay in a volume of 0.05 pc radius during 24 Myr. This is a strong argument favoring the bound nature of the V1311 Ori system. In contrast, star E (RX J0534.0-0221) is an unbound member of the YMG, separated from V1311 Ori along the line of sight by 4 pc. The RV of star E differs from the RVs of other stars by 1-2 km s^{-1}, so it could cover this distance in 2-4 Myr. However, in the tangential plane E is moving towards V1311 Ori, making it highly unlikely that E was ejected from this system a few Myr ago.

5. DISCUSSION AND SUMMARY

The family of V1311 Ori is a gravitationally bound system containing six low-mass PMS stars. Its spatial motion is similar to the BPMG and THOR moving groups, so V1311 Ori originated from the same star-formation region some 24 Myr ago. Fast rotation of some stars, their location on the CMD, chromopsheric and X-ray emission match the young age.

Although the Gaia parallaxes and PMs of the brightest stars A and B are biased by subsystems, the internal motions inferred from astrometry appear to be slow and do not contradict the bound nature of this system of ∼10 kau size. Its structure, however, is not clear. The projected separations between A, BC, and D are comparable (Figure 1), so it could be a dynamically unstable configuration, in other words a mini-cluster. The estimated crossing time on the order of 1 Myr suggests that the system has survived until now, but may evolve in the future owing to dynamical interactions between its members. One or both lowest-mass stars C and D might be ejected, leaving a stable hierarchy with 4-5 components. The tight inner pairs Aa,Ab and Ba,Bb will not be affected. Alternatively, this system could be already dynamically stable, with a hierarchy described by Fig-

ure 2, if star D is closer by >15 kau than ABC. Other configurations (for example, two triples Aa,Ab-D and Ba,Bb-C) are not excluded, but appear less likely.

The V1311 Ori system was discovered in the search for wide hierarchies within 100 pc (Tokovinin 2022). Some low-mass wide triples in the field also have non-hierarchical configurations with comparable separations. Admittedly, a stable triple can appear non-hierarchical due to projection, but statistical analysis of all these systems demonstrates that many are indeed just above the stability limit. They witness early dynamical interactions in unstable hierarchies and represent the surviving population. The system V1311 Ori illustrates the transition from assembly to dispersal.

Gagné et al. (2021) establish the relation between BPMG and THOR groups and believe that they were formed together, as well as the Kounkel & Covey's groups Theia 62 and 65. The large size of the V1311 Ori system (∼10 kau) speaks against its formation in a dense environment. Small masses of these M-dwarfs do not favor binary formation by disk fragmentation (Kratter & Lodato 2016). So, the architecture of this and other similar low-mass hierarchies reflects only three basic processes involved in the formation of stellar systems: fragmentation, accretion, and internal dynamics, while disk fragmentation and dynamical interactions with other cluster members are irrelevant. Fragmentation and collapse begin in the densest parts of the parent cloud (Vázquez-Semadeni et al. 2019), and these first stars have a larger supply of gas, compared to stars formed later at the periphery. An accreting binary shrinks while its mass ratio increases. The inner and most massive subsystems Aa,Ab and Ba,Bb in V1311 Ori with large mass ratios were likely the first to form. Stars C and D, formed later, have smaller masses. They could be gravitationally bound to A and B from the outset if the internal motions in the parent cloud were slow, or became bound as they approached and got captured on wide orbits, possibly with assistance of the remaining gas around A and B. As a result, the system of V1311 Ori is mass-segregated, resembling a young custer. In fact, it is (or was) a cluster with a small number of stars. Other wide low-mass marginally stable triples in the field could be the remnants of similar mini-clusters. They also appear mass-segregared (in two thirds of those triples, the most massive star belongs to the inner pair).

This work is devoted to the structure and dynamics of the V1311 Ori system. The physics of these young low-mass stars is outside its scope, but it is definitely worth further study. Being members of a coeval group with a well-measured distance, they are more interesting than simple stars or binaries. Measuring stellar masses from the orbits of Aa,Ab and Ba,Bb is an obvious prospect.

The research was funded by the NSF's NOIRLab. This work used the SIMBAD service operated by Centre des Données Stellaires (Strasbourg, France), bibliographic references from the Astrophysics Data System maintained by SAO/NASA. This work has made use of data from the European Space Agency (ESA) mission Gaia (https://www.cosmos.esa.int/gaia), processed by the Gaia Data Processing and Analysis Consortium (DPAC, https://www.cosmos.esa.int/web/gaia/dpac/consortium). Funding for the DPAC has been provided by national institutions, in particular the institutions participating in the Gaia Multilateral Agreement. This paper includes data collected by the TESS mission funded by the NASA Explorer Program. The data were obtained through the Barbara A. Mikulski Archive for Space Telescopes (MAST) at the Space Telescope Science Institute. The specific observations analyzed can be accessed via 10.17909/t9-nmc8-f686. This research has made use of the services of the ESO Science Archive Facility (FEROS spectra, ESO programs 094.A-9002 and 089.A-913).

Facility: SOAR, CTIO:1.5m, Gaia, TESS

REFERENCES

Alonso-Floriano, F. J., Caballero, J. A., Cortés-Contreras, M., Solano, E., & Montes, D. 2015, A&A, 583, A85,

Bell, C. P. M., Mamajek, E. E., & Naylor, T. 2015, MNRAS, 454, 593,

Bell, C. P. M., Murphy, S. J., & Mamajek, E. E. 2017, MNRAS, 468, 1198,

Bressan, A., Marigo, P., Girardi, L., et al. 2012, MNRAS, 427, 127,

Caballero, J. A. 2010, A&A, 514, A98,

da Silva, L., Torres, C. A. O., de La Reza, R., et al. 2009, A&A, 508, 833,

Durkan, S., Janson, M., Ciceri, S., et al. 2018, A&A, 618, A5,

Elliott, P., & Bayo, A. 2016, MNRAS, 459, 4499,

Elliott, P., Bayo, A., Melo, C. H. F., et al. 2014, A&A, 568, A26,

Finch, C. T., Zacharias, N., Subasavage, J. P., Henry, T. J., & Riedel, A. R. 2014, AJ, 148, 119,

Fouqué, P., Moutou, C., Malo, L., et al. 2018, MNRAS, 475, 1960,
Gagné, J., Faherty, J. K., Moranta, L., & Popinchalk, M. 2021, ApJL, 915, L29,
Gagné, J., Mamajek, E. E., Malo, L., et al. 2018, ApJ, 856, 23,
Gaia Collaboration, Smart, R. L., Sarro, L. M., et al. 2021a, A&A, 649, A6,
Gaia Collaboration, Brown, A. G. A., Vallenari, A., et al. 2021b, A&A, 649, A1,
Høg, E., Fabricius, C., Makarov, V. V., et al. 2000, A&A, 355, L27
Janson, M., Hormuth, F., Bergfors, C., et al. 2012, ApJ, 754, 44,
Janson, M., Bergfors, C., Brandner, W., et al. 2014, ApJS, 214, 17,
Joncour, I., Duchêne, G., & Moraux, E. 2017, A&A, 599, A14,
Kounkel, M., & Covey, K. 2019, AJ, 158, 122,
Kratter, K., & Lodato, G. 2016, ARA&A, 54, 271,
Malo, L., Doyon, R., Lafrenière, D., et al. 2013, ApJ, 762, 88,
Mason, B. D., Wycoff, G. L., Hartkopf, W. I., Douglass, G. G., & Worley, C. E. 2001, AJ, 122, 3466,
Messina, S., Millward, M., Buccino, A., et al. 2017, A&A, 600, A83,
Paredes, L. A., Henry, T. J., Quinn, S. N., et al. 2021, AJ, 162, 176,
Rebull, L. M., Stauffer, J. R., Cody, A. M., et al. 2018, AJ, 155, 196,
Ricker, G. R., Winn, J. N., Vanderspek, R., et al. 2014, in Society of Photo-Optical Instrumentation Engineers (SPIE) Conference Series, Vol. 9143, Space Telescopes and Instrumentation 2014: Optical, Infrared, and Millimeter Wave, ed. J. Oschmann, Jacobus M., M. Clampin, G. G. Fazio, & H. A. MacEwen, 914320,
Skrutskie, M. F., Cutri, R. M., Stiening, R., et al. 2006, AJ, 131, 1163,
Stauffer, J., Collier Cameron, A., Jardine, M., et al. 2017, AJ, 153, 152,
Tokovinin, A. 2016a, Orbit: IDL Software For Visual, Spectroscopic, And Combined Orbits, Zenodo, doi: 10.5281/zenodo.61119
—. 2016b, AJ, 152, 11,
—. 2018, PASP, 130, 035002,
—. 2022, ApJ, in press (arXiv:2112.11943)
Tokovinin, A., Fischer, D. A., Bonati, M., et al. 2013, PASP, 125, 1336,
Vázquez-Semadeni, E., Palau, A., Ballesteros-Paredes, J., Gómez, G. C., & Zamora-Avilés, M. 2019, MNRAS, 490, 3061,
Vrijmoet, E. H., Henry, T. J., Jao, W.-C., & Dieterich, S. B. 2020, AJ, 160, 215,